Shock Tube Measurements and Kinetic Investigation on the Ignition Delay Times of Methane/Dimethyl Ether Mixtures

ARTICLE *in* ENERGY & FUELS · NOVEMBER 2012

Impact Factor: 2.79 · DOI: 10.1021/ef301339m

5 AUTHORS, INCLUDING:

Chenglong Tang
Xi'an Jiaotong University
72 PUBLICATIONS **740** CITATIONS
SEE PROFILE

Shaodong Niu
51 PUBLICATIONS **253** CITATIONS
SEE PROFILE

Zuohua Huang
Xi'an Jiaotong University
419 PUBLICATIONS **5,189** CITATIONS
SEE PROFILE

energy&fuels

Article

pubs.acs.org/EF

Shock Tube Measurements and Kinetic Investigation on the Ignition Delay Times of Methane/Dimethyl Ether Mixtures

Chenglong Tang, Liangjie Wei, Jiaxiang Zhang, Xingjia Man, and Zuohua Huang*

State Key Laboratory of Multiphase Flows in Power Engineering, Xi'an Jiaotong University, Xi'an 710049, People's Republic of China

Supporting Information

ABSTRACT: In this work, the ignition delay times of stoichiometric methane/dimethyl ether (DME) were measured behind the reflected shock waves over a wide range of conditions: temperatures between 1134 and 2105 K, pressures of 1, 5, and 10 bar, a DME blending ratio from 0 to 100% (M100 to M0), and an argon concentration of 95%. The present shock tube facility was validated by comparing the measured ignition delay times of DME with literature values and was used for measurement of the subsequent methane/DME ignition delay times. The ignition delay times of all mixtures exhibit a negative pressure dependence. For a given temperature, the ignition delay time of methane/DME decreases remarkably with the presence of only 1% DME. As the DME blending ratio increases, the ignition delay times are correspondingly decreased; however, the ignition promotion effect of DME is decreased. The calculated ignition delay times of methane/DME mixtures using two recently developed kinetic mechanisms are compared with those of measurements. The NUI C4 mechanism yields good prediction for the ignition delay time of methane. With an increase of the DME blending ratio, the performance of this model becomes moderated. Zhao's DME model yields good prediction for all of the mixtures studied in this work; thus, it was selected for analyzing the ignition kinetics of methane/DME fuel blends, through which the nonlinear effect of DME addition in promoting ignition is interpreted.

1. INTRODUCTION

Increasingly stringent emission regulations and inadequacy of fossil fuel supply drive the scientific investigations to find clean alternative fuels. Dimethyl ether (DME) is the simplest ether. DME can be produced through a variety of resources such as coal, oil residual, or biomass. The physical properties of DME are similar to those of liquid petroleum gas, which facilitates easier and safer onboard transportation.[1] Because DME has no C−C bond and high oxygen content, the combustion of DME can achieve almost soot-free emission. Thus, DME has recently been emerging as a promising substitute for natural gas and liquid petroleum gas.

Practically, DME has excellent autoignition characteristics because of its high cetane number, and it has been used as an ignition enhancer for methanol-fueled engines.[2] Recent researches[3−8] showed that when diesel engines are fueled with DME/diesel blends, spray atomization is improved, which leads to better combustion performances. Soot emission is significantly reduced and NO_x is decreased to a certain extent while CO and HC emissions are only slightly increased with an increase of the DME blending ratio in the fuel blends. Additionally, the feasibility of using DME as an ignition timing control method in HCCI engines has been examined,[9,10] and results reveal that the ignition timing can be controlled by the quantity of the DME supply but the rapidity of combustion cannot be manipulated. Furthermore, the potential problems for DME fueling in gas turbines for power generation have also been evaluated,[11−13] and results show that firing DME yields lower combustion instability and less NO_x and CO emissions. Fundamentally, the low-pressure laminar premixed flame structures of stoichiometric and rich DME/air flames have been sampled to identify the reaction paths of DME combustion through molecular beam photoionization mass spectrometry.[14,15] The laminar flame speeds of DME/air mixtures were measured by using a variety of experimental techniques.[16−19] Dagaut et al.[20] studied the oxidation of DME in a jet-stirred reactor at 10 atm and in the temperature range between 550 and 1100 K. Oxidation and/or pyrolysis of DME was also investigated in flow reactors, at both low[21] and high temperatures,[22] and in a shock tube.[23]

The autoignition characteristics of DME have also been extensively investigated.[24−26] Specifically, Pfahl et al.[24] studied the autoignition process of DME/air in a shock tube at high pressure and low-to-intermediate temperatures, which are relevant to the actual engine conditions. They found that the DME autoignition behavior is similar to that of *n*-heptane, and a two-step autoignition process at low temperatures and a negative temperature coefficient (NTC) behavior was recognized. Subsequently, Mittal et al.[25] measured the ignition delay time of $DME/O_2/N_2$ mixtures at elevated pressure (10−20 bar) and relatively low temperature (615−735 K) in a rapid compression machine, and a two-step self-ignition and NTC of DME were also observed. This behavior becomes more prominent for the low-pressure and oxygen-lean mixtures. Dagaut et al.[20] and Cook et al.[26] measured the ignition delay times of DME in argon-diluted oxygen at high temperatures behind the reflected shock waves.

Natural gas has been widely used in spark ignition engines because of its high resistance to knock, low pollutant emission, and low cost. Natural gas is also a primary fuel for power-generation gas turbines. Methane is the main component of natural gas. Previous literature[27−29] shows that methane has

Received: August 13, 2012
Revised: October 24, 2012
Published: October 25, 2012

autoignition characteristics vastly different from those of DME. Thus, the addition of DME into methane is expected to alter the ignition characteristics of methane. Several studies have already attempted to study the autoignition characteristics of methane/DME mixtures. Amano and Dryer[30] investigated the effect of adding a small amount of DME on the oxidation chemistry of methane related to the ignition process in a flow reactor. Because they use an electrical-resistance-type air heater, the temperature is inherently limited on the order of 1000 K. Additionally, the reaction time can only be indirectly calculated from the axial distance from the mixing to the sampling location and the onset of ignition is difficult to well-define in the flow reactor, so the ignition delay times of the methane/DME mixtures were not reported in ref 30. Chen et al.[31] numerically studied the effects of adding DME on the ignition characteristics of methane/air mixtures, but these calculations were only conducted at several fixed temperatures. There have also been some investigations on the HCCI combustion characteristics of methane/DME mixtures.[9,10]

There are several objectives in the present work. First, the goal is to provide ignition delay time data for the methane/DME mixtures over a wide range of experimental conditions. The ignition delay times of pure DME will be measured and compared with previous literature values so as to validate our experimental apparatus, which is subsequently used for measurements of methane/DME mixtures. Second, although several kinetic models for DME oxidation and combustion have been proposed,[20,32,33] these models have not yet been validated against the ignition delay time data of DME or methane/DME mixtures up to 10 bar; thus, another objective of the present work is to compare the computations from these models with the experimental measurements. Finally, kinetic investigation on the ignition chemistry through sensitivity analysis and species concentration profiles will be conducted and the effects of the DME blending ratio on the ignition delay time will be discussed.

2. EXPERIMENTAL PROCEDURES AND NUMERICAL APPROACHES

2.1. Setup and Procedures. Details of the shock tube facility were described in ref 34, and only a brief introduction is given here. The shock tube consists of a 2-m-long driver section (high-pressure helium) and a 7.3-m-long driven section (low-pressure test mixture) with a diameter of 11.5 cm. Between them, there is a connecting flange (0.06 m long) with diaphragms on both sides for separation of the driver and driven sections. Before each experiment, the whole tube is evacuated to a pressure below 10^{-4} Torr. After the mixtures are prepared, the rupture of the diaphragm is triggered by evacuating the small volume of the flange section, and a shock wave is then generated. Four fast-response sidewall pressure transducers (PCB 113B26) are located along the end part of the driven section with equal distance (300 mm) apart. The last sidewall pressure transducer is located at 2 cm apart from the endwall. The endwall pressure and CH* emission signal are respectively detected by an endwall pressure transducer (PCB 113B03) and photomultiplier (Hamamatsu CR 131) with a 430 ± 10 nm filter. All pressure transducers are shielded with silicone rubber to minimize the heat-transfer effect. Three time counters (Fluke PM 6690) are used to measure the time intervals between the instants of shock arrival at each sidewall-pressure-transducer location, with which the speed of the shock wave at the endwall is determined by linear extrapolation of the axial velocity profile to the endwall. Typical attenuation rates of incident shock are less than 3%. The conditions behind the reflected shock wave are calculated by the chemical equilibrium program *GasEq*,[35] assuming frozen chemistry, with the thermodynamic data included in *GasEq*.[35] The uncertainties of the temperature behind the reflected shock waves are less than 25 K and result in an uncertainty of the measured ignition delay times of less than 10%.

Reactant mixtures are prepared in a 128 L stainless steel tank by partial pressure law at room temperature and are allowed to settle overnight before the experiment. The purities of oxygen (O_2), argon (Ar), DME, and methane are higher than 99.995%, 99.995%, 99.5%, and 99.995%, respectively. Table 1 gives detailed mixture compositions for all test conditions. All fuel/O_2/Ar mixtures, at stoichiometric and 3.76 Ar/O_2 ratios, are diluted in argon (20% mixture + 80% argon).

Table 1. Mixture Compositions in the Study (ϕ = 1.0 for All Seven Mixtures)

mixture	blend	X_{CH_4}	X_{DME}	X_{O_2}	X_{Ar}
1-M100	100% CH_4/0% DME	1.901	0.0	3.802	94.297
2-M99	99% CH_4/1% DME	1.874	0.019	3.804	94.303
3-M95	95% CH_4/5% DME	1.766	0.093	3.811	94.330
4-M90	90% CH_4/10% DME	1.637	0.182	3.820	94.362
5-M80	80% CH_4/20% DME	1.395	0.349	3.835	94.421
6-M50	50% CH_4/50% DME	0.775	0.775	3.876	94.574
7-M0	0% CH_4/100% DME	0.0	1.309	3.927	94.764

2.2. Data Validation. Up to now, Dagaut et al.[20] and Cook et al.[26] have studied the ignition delay times of argon-diluted DME up to a pressure of 6.6 bar. The gas composition containing 1% DME in a mixture that is similar to that of researches[20,26] is chosen to validate the ignition delay time measurements in the study. Figure 1 gives examples of the determinations of the ignition delay times in this work. As described above, the endwall pressure and endwall CH* emission are respectively employed in parts a and b of Figure 1. The ignition delay time is defined as the time interval between the incident shock wave arrival at the endwall and the onset of the ignition event, which is defined by extrapolation of the maximum slope line of the endwall pressure or CH* emission profile to the baseline. It is noted that, because of the facility-dependent nonideal gas dynamics, there has been an observable pressure rise in the ignition process, as shown in Figure 1, which will lead to an increase of the temperature to a certain extent. However, because the temperature studied here lies in the range between 1100 and 2100 K and most of the ignition delay times measured in this study are less than 2 ms, the pressure rise does not necessarily affect the accuracy of the present ignition delay time measurements.

Figure 2 shows a comparison between the current measured data and those in the literature.[20,26] Experimental data are all normalized to 3.5 bar with a pressure index of −0.66, which was suggested by Cook et al.[26] The ignition delay times measured by the endwall pressure or CH* emission agree fairly well over the temperature range covered. Thus, either the endwall pressure or endwall CH* emission can be used to obtain the ignition delay times. Compared with Cook et al.,[26] the agreement is fairly good below 1333 K (≈1000 K/T = 0.75). However, when the temperature exceeds 1333 K, Cook et al.'s data exhibit lower ignition delay times. The ignition delay times were obtained by sidewall emission or pressure in Cook et al.'s

dx.doi.org/10.1021/ef301339m | *Energy Fuels* 2012, 26, 6720−6728

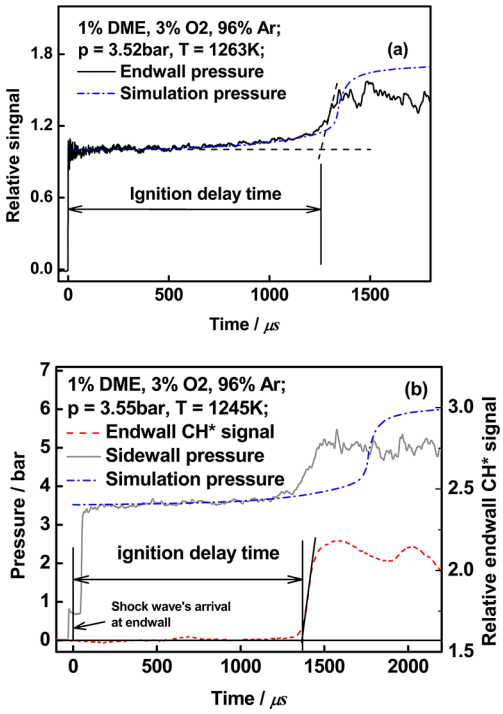

Figure 1. Examples of ignition delay time definitions in the current work: (a) endwall pressure profile determination; (b) endwall CH* emission profile determination.

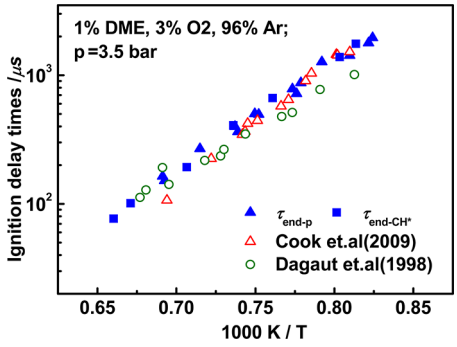

Figure 2. Comparison of the current experimental results with the literature data.

work.[26] Horning et al.[36] and Petersen[37] have discussed the discrepancies existing in the ignition delay time measurements by using endwall and sidewall positions. When the temperature is relatively high and the ignition delay time is short, this discrepancy becomes more noticeable.[37] Figure 3 gives a comparison between those of Cook et al.[26] and the ignition delay time measured at the sidewall at the same position as Cook et al.'s measurement. Good agreement is achieved in Figure 3. This added support to the discrepancy analysis. In Dagaut et al.'s work,[20] the endwall CO_2 emission was used to determine the ignition delay time. In the high-temperature and short-ignition-delay time region, good agreement is achieved between Dagaut et al.[20] and this work. However, Dagaut et al.'s work[20] gives relatively lower ignition delay times in the lower temperature range; thus, Dagaut's work exhibits lower activation energy in this range. This is attributed to the smaller-diameter shock tube used in Dagaut et al.'s work. Petersen[38] and Davidson and Hanson[39] interpreted the influence of the shock tube diameter on the activation energy,

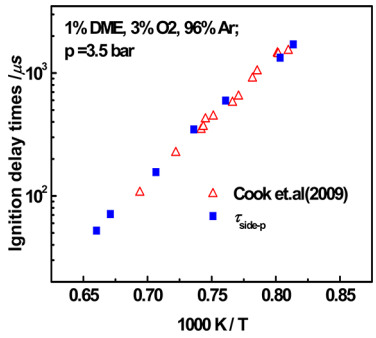

Figure 3. Comparison of the ignition delay measurement at 2 cm from the sidewall of the current work and Cook et al.[26]

and they found that a smaller diameter gives a lower activation energy because of the more profound boundary layer effect.

2.3. Kinetic Model for DME Oxidation. The *SENKIN*[40] module in the *Chemkin II*[41] package was used to calculate the ignition delay time, assuming a zero-dimensional, constant-volume adiabatic model. The onset of ignition is defined as the instance with the maximum pressure rise rate during kinetic simulation.

There have been several studies on the oxidation kinetics of DME. Specifically, Dagaut et al.[20] proposed a detailed reaction mechanism based on shock-tube and JSR experimental data. Fischer et al.[22] and Curran et al.[21] studied the reaction kinetics of DME from low to high temperature and pressures up to 18 atm. Zhao et al.[32] theoretically studied the thermal decomposition of DME at different pressures and temperatures by the RRKM/master equation method, and a comprehensive DME kinetic model consisting of 55 species and 290 reactions was proposed and validated against the species profiles in the flow reactor, JSR species profiles, pyrolysis results, ignition delay times, and laminar flame speeds. Lowry et al.[33] updated the DME kinetic model (NUI-C4_49) to predict the laminar flame speed of the DME/methane blend based on the DME submechanism of Fischer et al.[21,22] and the C4 mechanism of NUI.[42,43]

It is expected that a well-developed kinetic model for methane/DME mixtures can give good predictions on the ignition delay times of methane and DME individually. Figure 4 shows a comparison among the measured ignition delay times of methane and DME and the calculations using Zhao's[32] and NUI-C4_49 models.[33] Figure 4a presents the measured and calculated ignition delay times for pure methane at pressures of 1, 5, and 10 bar. Because methane is the simplest hydrocarbon and its kinetic model has been well developed, computations from both models yield good agreement with the measurement. At a pressure of 1.0 bar, the computed ignition delay time by Zhao's model is slightly lower than that of NUI-C4_49, and excellent agreement is presented at 5 and 10 bar. At a pressure of 10 bar, because the temperature is lower than 1500 K, both models yield slightly higher ignition delay times than the measurements. Figure 4b shows the measured and calculated ignition delay times of DME at 1, 5, and 10 bar. Zhao's model shows excellent agreement with the measurements at the three pressures studied. The NUI-C4_49 model slightly underpredicts the ignition delay times at 1.0 bar, but as the pressure increases, the NUI-C4_49 model gives much lower ignition delay times than the measurements. Because Zhao's model is good at predicting the ignition delay time for both methane and DME, it is chosen to compute the ignition delay times for the

dx.doi.org/10.1021/ef301339m | *Energy Fuels* 2012, 26, 6720−6728

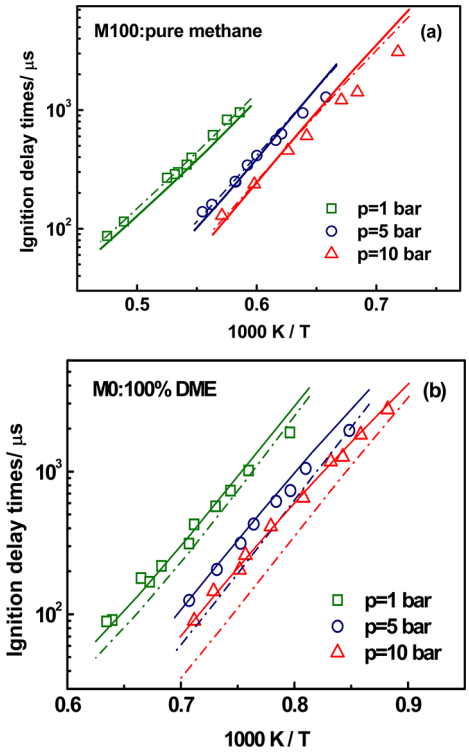

Figure 4. Comparison of Zhao's[32] and NUI c4_49[33] models for pure methane (a) and pure DME (b). Solid lines: Zhao et al.[32] Dash-dotted lines: NUI c4_49.[33]

methane/DME fuel mixtures and subsequent kinetic mechanism study.

3. RESULTS AND DISCUSSION

Ignition delay times of methane/DME fuel blends with DME blending ratios of 0%, 1%, 5%, 10%, 20%, 50%, and 100% were measured in the study at 1, 5, and 10 bar.

For all mixtures, the ignition delay times show a strong Arrhenius dependence on the pressure and temperature. A multiregression analysis was conducted, and the ignition delay time is correlated with the experimental parameters as follows:

$$\tau = Ap^n \exp(E/RT) \quad (1)$$

where τ is the ignition delay time (μs), A and n are correlation parameters, p is the pressure (bar), T is temperature (K), E is the overall activation energy (kcal/mol), and $R = 1.986 \times 10^{-3}$ kcal/(mol·K) is the universal gas constant. The ignition delay times for all mixtures give a negative dependence on the pressure, and the overall activation energy decreases with increasing DME blending ratio, as shown in Table 2. Because the residual squares for all mixtures in multiregression analysis are over 0.98, the above empirical correlation is expected to capture the experimental data with high fidelity.

Table 2. Correlation Parameters for DME/Methane Mixtures

mixture	A	n	E(kcal/mol)	R^2
1-M100	3.582×10^{-3}	−0.737	42.5 ± 0.6	0.995
2-M99	3.899×10^{-3}	−0.655	40.6 ± 1.1	0.981
3-M95	2.098×10^{-3}	−0.539	40.0 ± 0.7	0.992
4-M90	1.784×10^{-3}	−0.530	39.1 ± 0.8	0.990
5-M80	9.159×10^{-4}	−0.535	39.4 ± 0.6	0.994
6-M50	5.993×10^{-4}	−0.544	38.4 ± 0.6	0.995
7-M0	3.927×10^{-4}	−0.585	38.5 ± 0.6	0.994

3.1.. Effect of the Blending Ratio on the Ignition Delay Times. Figure 5 shows the measured and computed ignition

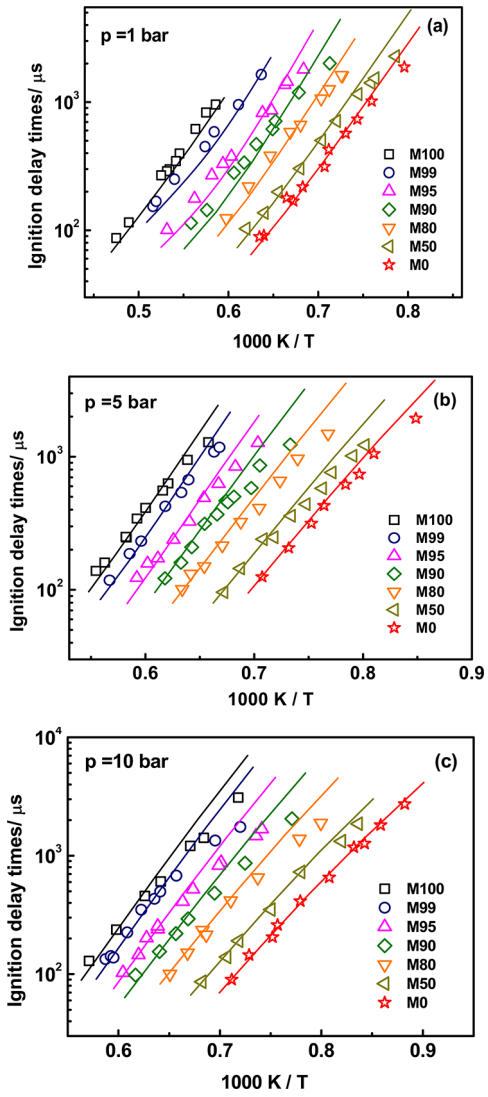

Figure 5. Comparisons of experimental data with Zhao et al.'s[32] DME model predictions for various methane/DME blends at different pressures.

delay times for all mixtures at pressures of 1, 5, and 10 bar. Numerical predictions using Zhao's model agree well with the measurements. All data sets show a similar dependence on the temperature: the logarithmic ignition delay time is a linear function of the inverse temperature.

Figure 6 shows the ignition delay times as a function of the DME blending ratio for different pressures (a) and different temperatures (b). It is noted that the experimental schemes do not cover all data points in the isobaric curves in Figure 6a and in the isothermal curves in Figure 6b, so some of the data in Figure 6 are obtained through eq 1. Computations with Zhao's model show excellent agreement with eq 1 correlations. With increasing DME blending ratio, the ignition delay time initially experiences a steep decrease and then gradually a decreasing

dx.doi.org/10.1021/ef301339m | Energy Fuels 2012, 26, 6720−6728

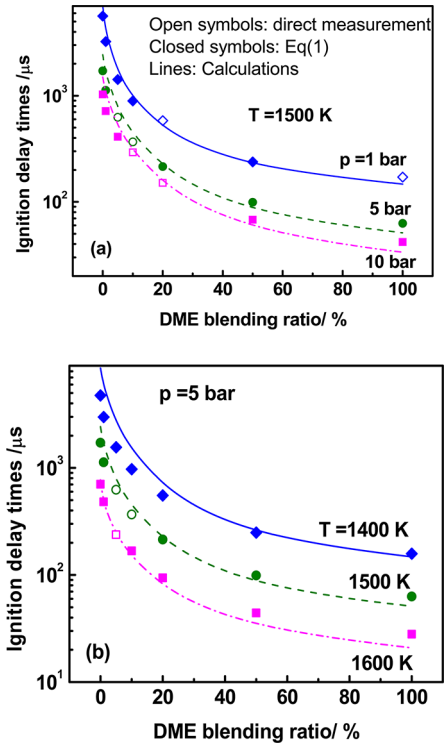

Figure 6. Ignition delay times as a function of the DME blending ratio: (a) different pressures; (b) different temperatures.

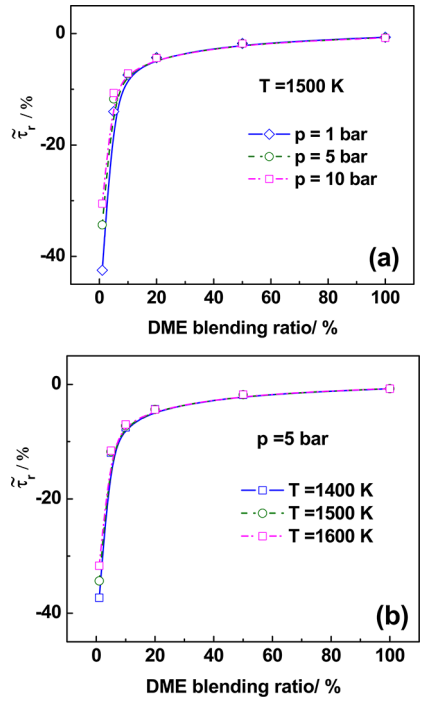

Figure 7. Normalized ignition delay time reduction parameter versus the DME blending ratio: (a) different pressures; (b) different temperatures.

trend. Increases in the pressure or temperature reduce the ignition delay time for all mixtures.

To quantitatively illustrate the effect of the DME blending ratio on the ignition delay time for all mixtures, a normalized ignition delay time reduction parameter, $\tilde{\tau}_r$, which illustrates the sensitivity of the ignition delay time to the DME blending ratio, is defined as

$$\tilde{\tau}_r = \frac{\tau_{X_{DME}} - \tau_{CH_4}}{\tau_{CH_4}} \times 100\% \quad (2)$$

where X_{DME} is the DME blending ratio, $\tau_{X_{DME}}$ is the ignition delay time at the DME blending ratio of X_{DME}, and τ_{CH_4} is the ignition delay time of pure methane fuel. Figure 7 depicts the effect of the blending ratio on $\tilde{\tau}_r$ at the conditions corresponding to Figure 6. The ignition delay time reduction parameters exhibit a similar dependence on the DME blending ratio. For a DME blending ratio of 1%, $\tilde{\tau}_r$ is higher than 30%, indicating that a 1% DME presence will decrease the ignition delay time by 30%. When the DME blending ratio is over 50%, $\tilde{\tau}_r$ is less than 10%, indicating that doubling the DME blending ratio only results in an ignition delay time reduction of less than 5%. Parts a and b of Figure 7 show that, for a DME blending ratio less than 5%, $\tilde{\tau}_r$ is higher at low pressures and temperatures. However, at high DME blending ratios, $\tilde{\tau}_r$ is insensitive to variations of either the pressure or temperature. This implies that the effect of DME addition on the ignition delay time reduction is facilitated at lower pressures and temperatures.

3.2. Chemical Kinetic Analysis. To understand the ignition chemistry of methane/DME fuel blends, sensitivity analysis and free-radical mole fraction analysis were performed with Zhao et al.'s DME model.[32]

3.2.1. Sensitivity Analysis. Sensitivity analysis on the ignition delay times of methane/DME fuel blends with various DME blending ratios was performed to ascertain the important reactions in the ignition regime. The sensitivity index is calculated by perturbing the reaction rate, defined as

$$S_i = \frac{\tau(2k_i) - \tau(0.5k_i)}{1.5\tau(k_i)} \quad (3)$$

where S_i is the ignition delay time sensitivity, τ is the ignition delay time, and k_i is the rate of the ith reaction in the kinetic mechanism. Negative sensitivity indicates an increase in the rate constant of the reaction, resulting in a reduction in the ignition delay times and thus increasing the overall reactivity and vice versa. Figure 8 depicts the 17 most important sensitive reactions for mixtures **M0**, **M1**, **M10**, **M50**, and **M100** at a temperature of 1400 K and a pressure of 10 bar.

For a pure methane mixture (**M100**), the chain-branching reaction R1, H + O_2 = O + OH, has the highest negative sensitivity index, indicating that reaction R1 is the most important reaction that dominates the ignition. The ignition delay time is sensitive to several chain-branching reactions involving the methyl radical, including R49, CH_3 + O_2 = CH_3O + O, and R50, CH_3 + O_2 = CH_2O + OH. The chain propagation reaction R51, CH_3 + HO_2 = CH_3O + OH, in which the less reactive methyl radical is consumed to produce a more reactive OH radical, has a sensitivity index comparable to those for R49 and R50; thus, R51 increases the system reactivity. Methyl radical recombination reaction R52, CH_3 + CH_3(+M) = C_2H_6(+M), removes the methyl radical from the radical pool, and it is the most important ignition inhibition reaction. The hydrogen abstraction reaction R54, CH_4 + H = CH_3 + H_2, competes with reaction R1 for a hydrogen radical, and it has a comparably high positive sensitivity index for R54. The hydrogen abstraction from molecular methane by OH

dx.doi.org/10.1021/ef301339m | *Energy Fuels* 2012, 26, 6720−6728

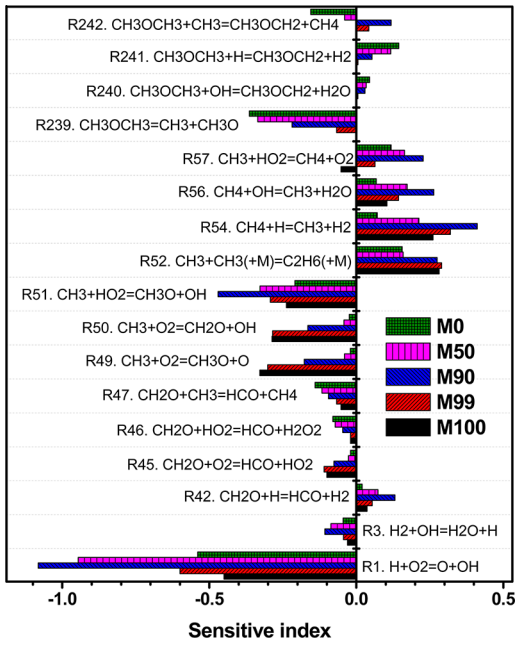

Figure 8. Normalized sensitivity of the ignition delay for various DME blending ratios at ϕ = 1.0, T = 1400 K, and p = 10 bar.

radical attack also has an inhibition effect on the ignition. This sensitivity diagram for methane reveals the fact that most of the high sensitivity reactions involve the consumption of a methyl radical, indicating its importance in radical pool growth and hence the ignition process.

In pure DME mixture (**M0**), reaction R1 still has the highest negative sensitivity index. The unimolecular decomposition reaction R239, $CH_3OCH_3 = CH_3 + CH_3O$, is another ignition-promoting reaction. R239 accelerates the ignition because it yields methyl and methoxy radicals, which are the major initial sources of radicals. The methoxy radical is highly reactive, and it then quickly decomposes to produce a formaldehyde molecule by reaction R71, $CH_3O + M = CH_2O + H + M$. The methyl radical generated through DME decomposition subsequently acts as an attacker to abstract H from the DME molecule and to form the CH_3OCH_2 radical through reaction R242, $CH_3OCH_3 + CH_3 = CH_3OCH_2 + CH_4$. When the methyl and HO_2 radical concentrations increase, reaction R51 becomes increasingly important in radical pool growth. Furthermore, the methyl radical also participates in reaction R47, $CH_2O + CH_3 = HCO + CH_4$, to yield a formyl radical, and it has a negative sensitivity index, thus promoting DME ignition. The main ignition inhibition reaction includes the chain termination reaction R52 and hydrogen abstraction reaction R241, $CH_3OCH_3 + H = CH_3OCH_2 + H_2$.

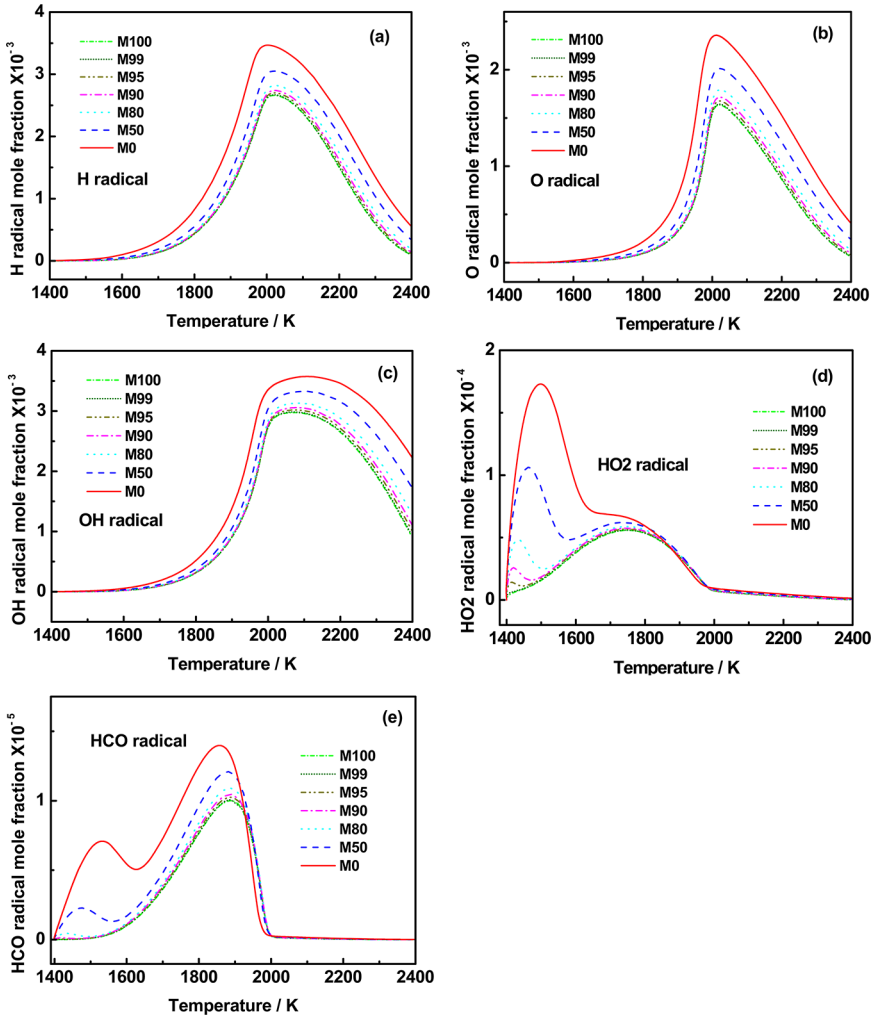

Figure 9. Mole fraction of free radicals for different DME blending ratios at ϕ = 1.0, T = 1400 K, and p = 10 bar.

dx.doi.org/10.1021/ef301339m | Energy Fuels 2012, 26, 6720−6728

When DME is present in methane, the ignition of methane is enhanced greatly because of the accelerated production of the methyl radical through decomposition of DME, as discussed above for a pure DME mixture. Another reason for the enhanced reactivity by DME addition is as follows. For a pure methane mixture (**M100**), oxidation of the methyl radical is mainly by reaction with molecular oxygen, and these reactions have high activation energy, thus controlling the slow ignition. As DME is added, a relatively large amount of the HO_2 radical can be produced, oxidation of CH_3 is accelerated through R51, and the ignition is consequently promoted.

It is noted that R57, $CH_3 + HO_2 = CH_4 + O_2$, shows promotion reactivity for a 100% CH_4 mixture. At the initial step of radical pool growth, production of the methyl radical is dominated by the reverse reaction of R57.[31] In contrast, radical recombination with the methyl and hydroperoxyl radicals is disadvantaged at the initial stage before the radicals reach sufficiently high concentration. Thus, reaction R57 gives a slight promotion effect for pure methane. However, as DME is added, the methyl radical is more rapidly produced through DME decomposition, and reaction R57 consumes the methyl and hydroperoxyl radicals, thus playing an inhibition role on ignition.

The sensitivity indices of reactions R49 and R50 decrease with increasing DME blending ratio, and reaction R239 becomes more prominent in radical pool buildup as the DME blending ratio increases.

3.2.2. Small Radical Mole Fraction Analysis. Free radicals including H, O, OH, HO_2, and CH_3 act as chain carriers, and their evolution profiles are important for an understanding of the ignition chemistry. The mole fraction profiles of these radicals are plotted to further interpret the effect of DME addition to methane oxidation radical pool growth in a homogeneous ignition system.

Figure 9 presents the mole fraction of H, O, and OH radicals for all mixtures at a pressure of 10 bar and a temperature of 1400 K. The results show that the concentrations of H, O, and OH radicals at various DME blending ratios peak at around 2000 K. With an increase of the DME fraction, the concentrations of these radicals increase, resulting in an enhancing effect on the system reactivity and decreasing ignition delay times. Concentration profiles of the HO_2 radical are shown in Figure 9d. For a pure methane mixture (**M100**), the peak concentration of the HO_2 radical appears at a temperature of 400 K higher than the initial gas temperature of the system, which is typically defined as the onset of ignition. As the DME blending ratio increases, another HO_2 concentration peak arises at an earlier stage of the ignition process (or low temperature). The reason is that formaldehyde is more easily available for DME than that in methane during ignition as reactions R239 and R248. Formaldehyde undergoes hydrogen abstraction by H and OH to yield HCO. When the HCO radical reaches a sufficiently high concentration, it reacts with a O_2 molecule to form the HO_2 radical through reaction R31, $HCO + O_2 = CO + HO_2$. Figure 9e illustrates the mole fraction of the formal radical for various DME blending ratios. Another peak in the HCO concentration profile is accordingly presented at an early stage when the DME blending ratio increases. In 100% DME, the first peaks of the HCO and HO_2 radicals appear at 1531 and 1499 K, respectively. When the methyl and HO_2 radical concentrations are sufficiently high, reaction R51 will become increasingly important in radical pool growth, yielding methoxy and OH radicals. Thus, the mole fraction of the HO_2 radical begins to decrease after the first peak. Formaldehyde, which is the main source of HCO radical formation, is almost consumed by H and OH radicals at an early stage, as shown in Figure 10, leading to a decrease in the HCO radical, which then decreases the mole fraction of the HO_2 radical.

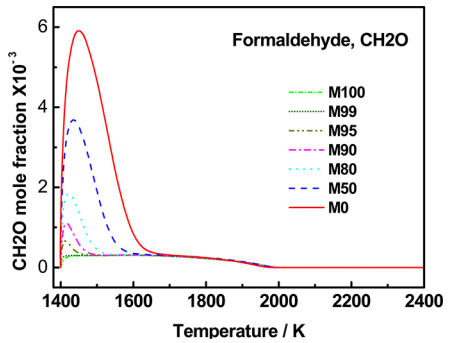

Figure 10. Mole fraction of formaldehyde (CH_2O) for different DME blending ratios at ϕ = 1.0, T = 1400 K, and p = 10 bar.

Figure 11 shows the mole fraction of the methyl radical versus the DME blending ratio at 10 bar and 1400 K. Increasing

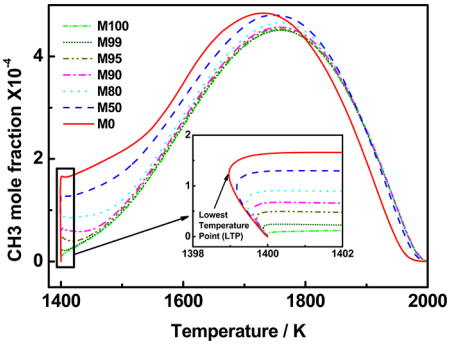

Figure 11. Mole fraction of the methyl radical for different DME blending ratios at ϕ = 1.0, T = 1400 K, and p = 10 bar.

the DME blending ratio increases the peak of the methyl racial concentration. At an early stage of radical pool buildup, methyl radicals increase steeply because of decomposition of DME, as shown in the inset. Through rate of production analysis at an early stage of ignition, production of the methyl radical is dominated by reaction R57 for **M100** mixtures. As the DME blending ratio increases, reactions R239 and R242 are becoming dominant for methyl radical production. At an early stage, unimolecular decomposition of fuels (methane and/or DME) dominates the radical pool buildup, and these reactions are endothermic; thus, the system temperature exhibits a weak decreasing trend. Subsequently, as the radical concentration increases, hydrogen-abstraction reactions become dominant in the fuel consumption, and the system temperature begins to increase. Thus, there is a lowest temperature point (LTP), which corresponds to the instant when the fuel decomposition reactions are being overtaken by the hydrogen-abstraction reactions. Figure 12 shows the methyl radical mole fraction at the LTP as a function of the DME blending ratio. With an increase in the DME blending ratio, the methyl radical concentration increases significantly at low DME blending ratios, but this effect is weakened at higher DME

dx.doi.org/10.1021/ef301339m | *Energy Fuels* 2012, 26, 6720−6728

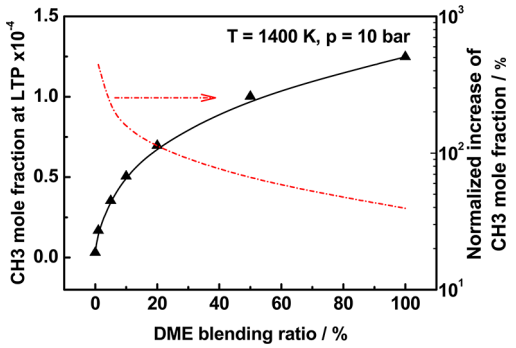

Figure 12. CH_3 radical mole fraction as a function of the DME blending ratio at the LTP.

blending ratios. The normalized increase in the CH_3 concentration is defined as

$$\frac{d[CH_3]/[CH_3]}{dX_{DME}} \times 100\% \quad (4)$$

where $[CH_3]$ is the mole fraction of the CH_3 radical at LTP.

As we see in Figure 12, this normalized increase of $[CH_3]$ is almost 300% for only a 1% DME blending ratio because, at the DME blending ratio, $[CH_3]$ is very small, and this parameter indicates that only 1% DME addition can lead to triplicity of $[CH_3]$. As the DME blending ratio increases to more than 20%, there is still some increase of $[CH_3]$, but at that point, $[CH_3]$ has already reached a sufficiently high value; thus, adding more DME is not as effective as it is in low-DME-blending-ratio cases. This behavior is consistent with variation of the ignition delay time and normalized ignition delay time reduction parameter, as shown in Figures 6 and 7, respectively.

To further illustrate the ignition promotion kinetics of DME addition during the initial radical pool buildup stage, Figure 13

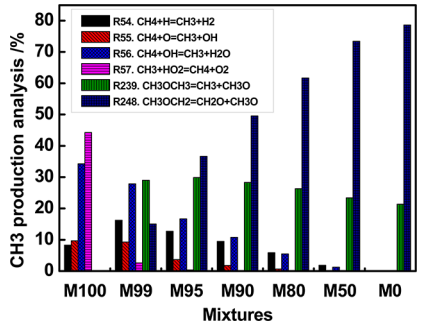

Figure 13. Total production of CH_3 radical analysis before the LTP.

lists six of the most important reactions and their corresponding contributions to the total production of CH_3 radicals before the LTP. For a pure methane mixture (**M100**), at an early stage, the methyl radical is mainly produced through the reverse reaction of R57. As the DME blending ratio increases, DME-related reactions R239 and R248 begin to dominate methyl radical production.

4. CONCLUSIONS

Ignition delay times of stoichiometric methane/DME fuel blends with DME blending ratios from 0% to 100% were measured using the shock tube. A kinetic study was conducted to interpret the ignition chemistry and the effect of the DME blending ratio on the ignition delay times. The main conclusions are summarized as follows: (1) Measured ignition delay times for various DME blending ratios are correlated with experimental parameters through eq 1 with high fidelity. Measured ignition delay times are compared with the model predictions, and excellent agreement is achieved by using Zhao et al.'s kinetic mechanism. (2) With increasing DME blending ratio, the ignition delay times initially decrease significantly, but for a DME blending ratio higher than 20%, this ignition delay time reduction effect by DME addition is weakened. (3) Chemical kinetic analysis shows that enhanced ignition of CH_4 by DME addition is attributed to an increase in the methyl radical concentration at an early stage of ignition, where fuel decomposition reactions dominate the ignition chemistry.

■ ASSOCIATED CONTENT

Ⓢ Supporting Information

Raw data of the ignition delay times. This material is available free of charge via the Internet at http://pubs.acs.org.

■ AUTHOR INFORMATION

Corresponding Author

*Telephone: 86-29-82665075. Fax: 86-29-82668789. E-mail: zhhuang@mail.xjtu.edu.cn.

Notes

The authors declare no competing financial interest.

■ ACKNOWLEDGMENTS

This work was supported by the National Natural Foundation of China (Grants 51136005 and 51121092) and the National Basic Research Program (Grant 2013CB228406).

■ REFERENCES

(1) Semelsberger, T. A.; Borup, R. L.; Greene, H. L. Dimethyl ether (DME) as an alternative fuel. *J. Power Sources* **2006**, *156* (2), 497−511.

(2) Karpuk, M. E.; Wright, J. D.; Dippo, J. L.; Jantzen, D. E. *Dimethyl ether as an ignition enhancer for methanol-fueled diesel engines*; SAE Technical Paper Series 912420; Society of Automotive Engineers: Warrendale, PA, 1991.

(3) Green, C. J.; Cockshutt, N. A.; KingL. *Dimethyl ether as a methanol ignition improver: substitution requirements and exhaust emissions impact*; SAE Technical Paper Series 902155; Society of Automotive Engineers: Warrendale, PA, 1990.

(4) Fleisch, T.; McCarthy, C.; Basu, A.; Udovich, C.; Charbonneau, P.; Slodowske, W.; Mikkelsen, S. E.; McCandless, J. *A new clean diesel technology: demonstration of ULEV emissions on a Navistar diesel engine fueled with dimethyl ether*; SAE Technical Paper Series 950061; Society of Automotive Engineers: Warrendale, PA, 1995.

(5) Yoon, H.; Yeom, K.; Bae, C. *The effects of pilot injection on combustion in dimethyl-ether (DME) direct injection compression ignition engine*; SAE Technical Paper Series 2007-24-0118; Society of Automotive Engineers: Warrendale, PA, 2007.

(6) Mohanan, P.; Kapilan, N.; Reddy, R. P. *Effect of diethyl ether on the performance and emission of a 4 - S Di diesel engine*; SAE Technical Paper Series 2003-01-0760; Society of Automotive Engineers: Warrendale, PA, 2003.

(7) Chapman, E. M.; Boehman, A. L.; Tijm, P.; Waller, F. *Emission characteristics of a Navistar 7.3L turbodiesel fueled with blends of dimethyl ether and diesel fuel*; SAE Technical Paper Series 2001-01-3626; Society of Automotive Engineers: Warrendale, PA, 2001.

(8) Wang, Y.; Li, G.; Zhu, W.; Zhou, L. Study on the application of DME/diesel blends in a diesel engine. *Fuel Process. Technol.* **2008**, *89* (12), 1272−1280.

(9) Konno, M.; Chen, Z. *Ignition mechanisms of HCCI combustion process fueled with methane/DME composite fuel*; SAE Technical Paper

Series 2005-01-0182; Society of Automotive Engineers: Warrendale, PA, 2005.
(10) Tsutsumi, Y.; Hoshina, K.; Iijima, A.; Shoji, H. *Analysis of the combustion characteristics of a HCCI engine operating on DME and methane*; SAE Technical Paper Series 2007-32-0041; Society of Automotive Engineers: Warrendale, PA, 2007.
(11) Glaude, P. A.; Fournet, R.; Bounaceur, R.; Moliere, M. DME as a potential alternative fuel for gas turbines: A numerical approach to combustion and oxidation kinetics. *ASME Conf. Proc.* **2011**, *2011* (54617), 649−658.
(12) Lee, M. C.; Seo, S. B.; Chung, J. H.; Joo, Y. J.; Ahn, D. H. Combustion performance test of a new fuel DME to adapt to a gas turbine for power generation. *Fuel* **2008**, *87* (10−11), 2162−2167.
(13) Lee, M. C.; Seo, S. B.; Chung, J. H.; Joo, Y. J.; Ahn, D. H. Industrial gas turbine combustion performance test of DME to use as an alternative fuel for power generation. *Fuel* **2009**, *88* (4), 657−662.
(14) Wang, J.; Chaos, M.; Yang, B.; Cool, T. A.; Dryer, F. L.; Kasper, T.; Hansen, N.; Kohse-Hoinghaus, K.; Westmoreland, P. R. Composition of reaction intermediates for stoichiometric and fuel-rich dimethyl ether flames: flame-sampling mass spectrometry and modeling studies. *Phys. Chem. Chem. Phys.* **2009**, *11* (9), 1328−1339.
(15) Cool, T. A.; Wang, J.; Hansen, N.; Westmoreland, P. R.; Dryer, F. L.; Zhao, Z.; Kazakov, A.; Kasper, T.; Kohse-Höinghaus, K. Photoionization mass spectrometry and modeling studies of the chemistry of fuel-rich dimethyl ether flames. *Proc. Combust. Inst.* **2007**, *31* (1), 285−293.
(16) Zhao, Z.; Kazakov, A.; Dryer, F. L. Measurements of dimethyl ether/air mixture burning velocities by using particle image velocimetry. *Combust. Flame* **2004**, *139* (1−2), 52−60.
(17) Daly, C. A.; Simmie, J. M.; Würmel, J.; Djebaïli, N.; Paillard, C. Burning velocities of dimethyl ether and air. *Combust. Flame* **2001**, *125* (4), 1329−1340.
(18) Qin, X.; Ju, Y. Measurements of burning velocities of dimethyl ether and air premixed flames at elevated pressures. *Proc. Combust. Inst.* **2005**, *30* (1), 233−240.
(19) Wang, Y. L.; Holley, A. T.; Ji, C.; Egolfopoulos, F. N.; Tsotsis, T. T.; Curran, H. J. Propagation and extinction of premixed dimethyl-ether/air flames. *Proc. Combust. Inst.* **2009**, *32* (1), 1035−1042.
(20) Dagaut, P.; Daly, C.; Simmie, J. M.; Cathonnet, M. The oxidation and ignition of dimethylether from low to high temperature (500−1600 K): Experiments and kinetic modeling. *Proc. Combust. Inst.* **1998**, *27*, 361−369.
(21) Curran, H. J.; Fischer, S. L.; Dryer, F. L. The reaction kinetics of dimethyl ether. II: Low-temperature oxidation in flow reactors. *Int. J. Chem. Kinet.* **2000**, *32* (12), 741−759.
(22) Fischer, S. L.; Dryer, F. L.; Curran, H. J. The reaction kinetics of dimethyl ether. I: High-temperature pyrolysis and oxidation in flow reactors. *Int. J. Chem. Kinet.* **2000**, *32* (12), 713−740.
(23) Hidaka, Y.; Sato, K.; Yamane, M. High-temperature pyrolysis of dimethyl ether in shock waves. *Combust. Flame* **2000**, *123* (1−2), 1−22.
(24) Pfahl, U.; Fieweger, K.; Adomeit, G. Self-ignition of diesel-relevant hydrocarbon−air mixtures under engine conditions. *Proc. Combust. Inst.* **1996**, *26* (1), 781−789.
(25) Mittal, G.; Chaos, M.; Sung, C. J.; Dryer, F. L. Dimethyl ether autoignition in a rapid compression machine: Experiments and chemical kinetic modeling. *Fuel Process. Technol.* **2008**, *89* (12), 1244−1254.
(26) Cook, R. D.; Davidson, D. F.; Hanson, R. K. Shock tube measurements of ignition delay times and OH time histories in dimethyl ether oxidation. *Proc. Combust. Inst.* **2009**, *32*, 189−196.
(27) Spadaccini, L. J.; Colket, M. B. Ignition delay characteristics of methane fuels. *Prog. Energy Combust. Sci.* **1994**, *20* (5), 431−460.
(28) de Vries, J.; Petersen, E. L. Autoignition of methane-based fuel blends under gas turbine conditions. *Proc. Combust. Inst.* **2007**, *31* (2), 3163−3171.
(29) Zhang, Y.; Huang, Z.; Wei, L.; Zhang, J.; Law, C. K. Experimental and modeling study on ignition delays of lean mixtures of methane, hydrogen, oxygen, and argon at elevated pressures. *Combust. Flame* **2012**, *159* (3), 918−931.
(30) Amano, T.; Dryer, F. L. Effect of dimethyl ethyl, NOx and ethane on CH_4 oxidation: High pressure, intermediate-temperature experiments and modeling. *Proc. Combust. Inst.* **1998**, *27* (1), 397−404.
(31) Chen, Z.; Qin, X.; Ju, Y. G.; Zhao, Z. W.; Chaos, M.; Dryer, F. L. High temperature ignition and combustion enhancement by dimethyl ether addition to methane−air mixtures. *Proc. Combust. Inst.* **2007**, *31*, 1215−1222.
(32) Zhao, Z.; Chaos, M.; Kazakov, A.; Dryer, F. L. Thermal decomposition reaction and a comprehensive kinetic model of dimethyl ether. *Int. J. Chem. Kinet.* **2008**, *40* (1), 1−18.
(33) Lowry, W. B.; Serinyel, Z.; Krejci, M. C.; Curran, H. J.; Bourque, G.; Petersen, E. L. Effect of methane−dimethyl ether fuel blends on flame stability, laminar flame speed, and Markstein length. *Proc. Combust. Inst.* **2011**, *33* (1), 929−937.
(34) Wei, L.; Tang, C.; Man, X.; Jiang, X.; Huang, Z. High-temperature ignition delay times and kinetic study of furan. *Energy Fuels* **2012**, *26* (4), 2075−2081.
(35) Morley, C. G. http://www.c.morley.dsl.pipex.com/, Aug 2010.
(36) Horning, D. C.; Davidson, D. F.; Hanson, R. K. Study of the high-temperature autoignition of *n*-alkane/O_2/Ar mixtures. *J. Propulsion Power* **2002**, *18* (2), 363−371.
(37) Petersen, E. L. Interpreting endwall and sidewall measurements in shock-tube ignition studies. *Combust. Sci. Technol.* **2009**, *181* (9), 1123−1144.
(38) Petersen, E. L.; Hanson, R. K. Nonideal effects behind reflected shock waves in a high-pressure shock tube. *Shock Waves* **2001**, *10* (6), 405−420.
(39) Davidson, D. F.; Hanson, R. K. Interpreting shock tube ignition data. *Int. J. Chem. Kinet.* **2004**, *36* (9), 510−523.
(40) Lutz, A. E.; Kee, R. J.; Miller, J. A. *SENKIN: A Fortran program for predicting homogeneous gas phase chemical kinetics with sensitivity analysis*; Sandia National Laboratories: Albuquerque, NM, 1988; SAND-87-8248.
(41) Kee, R. J.; Rupley, F. M.; Miller, J.*CHEMKIN-II: A FORTRAN Chemical Kinetics Package for the Analysis of Gas-Phase Chemical Kinetics*; Sandia National Laboratories: Albuquerque, NM, 1989; SAND89-8009B.
(42) Healy, D.; Donato, N. S.; Aul, C. J.; Petersen, E. L.; Zinner, C. M.; Bourque, G.; Curran, H. J. *n*-Butane: Ignition delay measurements at high pressure and detailed chemical kinetic simulations. *Combust. Flame* **2010**, *157* (8), 1526−1539.
(43) Healy, D.; Donato, N. S.; Aul, C. J.; Petersen, E. L.; Zinner, C. M.; Bourque, G.; Curran, H. J. Isobutane ignition delay time measurements at high pressure and detailed chemical kinetic simulations. *Combust. Flame* **2010**, *157* (8), 1540−1551.